International Journal of Research Studies in Management
2024 Volume 12 Number 15, 189-197

Longspan Xstyle Nielsen Tied Arch Bridge Static and Spatial Effects Score

Li, Mo ✉
Ningxia Communications Investment Group Co. Ltd., China (1720471793@qq.com)

Received: 25 September 2024
Revised: 5 November 2024
Accepted: 8 November 2024
Available Online: 8 November 2024
DOI: 10.5861/ijrsm.2024.1311

ISSN: 2243-7770
Online ISSN: 2243-7789

OPEN ACCESS

Abstract

This paper analyses the general idea of modelling the 128m main span Longspan Xstyle Nielsen Tied Arch Bridge, considers the construction process, and completes the spatial finite element static analysis of its deformation and force state for the whole bridge. The main work and innovative results are as follows: the spatial finite element analysis under constant load, live load and main force combination (constant load + live load) was completed for this bridge considering the construction process, and the spatial effect of the bridge was studied according to the results of the spatial finite element analysis. The results show that he vertical displacement and longitudinal stress of the girder are slightly unevenly distributed in the transverse direction, and the transverse stress is generally smaller than the longitudinal stress, which is mainly caused by the transverse prestressing force and the transverse component force of the boom. In addition to vertical displacement, the arch ribs also have slight transverse displacement.

Keywords: tied arch bridge, static analysis, spatial effect

Longspan Xstyle Nielsen Tied Arch Bridge Static and Spatial Effects Score

1. Project Description

Nielsen Tied Arch Bridge has attracted attention in the construction of large-span bridges due to its unique design and good mechanical properties. With the increase of span, its static and spatial effects are complicated, which requires higher design and construction requirements. This paper analyses the response of this bridge type under different working conditions and the spatial effects by establishing a mechanical model, aiming to provide theoretical and practical guidance for the design.

The main span of this bridge is 128m long, and its main arch rib is made of steel tubes with equal cross-section, which are filled with concrete to enhance its structural strength. The inclination angle of the steel pipe ribs is 9 degrees, which is not only aesthetically pleasing, but also effective in spreading out and carrying the loads on the bridge. In addition, the bridge is equipped with 56 diagonal booms, which play an important role in supporting and stabilizing the bridge structure. The main girder is a fully prestressed concrete structure with a single box and three chambers. This structural design provides the bridge with higher stability and durability when subjected to loads. Since the structural design and force state of the bridge are very complicated, precise calculation and strict control are required during the design and construction process to ensure the safety and reliability of the bridge. The design of the whole bridge takes into full consideration of the mechanical principles and practical use requirements, and strives to achieve the best balance between aesthetics, practicality and economy.

2. The basic principle of finite element method

(1) Displacement function selection

Node displacement calculation formula:

$$\{u\}=[N]\{\delta\}^e \quad (1)$$

In equation (1): $\{\delta\}^e$ denotes the node displacement matrix; $\{u\}$ denotes the cell displacement matrix; $[N]$ denotes the shape function matrix.

(2) Unit stiffness matrix

The functional equation for the unit strain is derived from the displacement formula of the node:

$$\{\varepsilon\}=[G]\{u\}=[G][N]\{\delta\}^e=[B]\{\delta\}^e \quad (2)$$

In equation (2), $\{\varepsilon\}$ is the unit strain matrix; $[B]$ is the strain matrix of the unit node. The functional equation for the unit stress is derived from the physical relationship:

$$\{\sigma\}=[D]\{\varepsilon\}=[D][B]\{\delta\}^e \quad (3)$$

In equation (3), $[D]$ denotes elasticity coefficient matrix; $\{\sigma\}$ denotes unit stress matrix. Functional equation between unit node force and node displacement:

$$\{f\}^e=\{k\}\{\delta\}^e \quad (4)$$

In equation (4): $\{k\}$ denotes the unit stiffness matrix; $\{f\}^e$ denotes the equivalent nodal force matrix of the unit. Convertible:

$$\{k\}^e = \int [B]^T [D][B] dx \quad (5)$$

(3) Derive the overall stiffness matrix of the structure

The element stiffness matrix is obtained by direct stiffness method $\{k\}^e$ Combine the unit equivalent nodal force matrix into the overall stiffness matrix $[k]$, and combine the unit equivalent nodal force matrix into the total load column matrix, while the boundary conditions need to be considered in order to limit the movement of the rigid body $[F]$, the calculation formula is as follows:

$$\{F\} = [K]\{\delta\} \quad (6)$$

In equation (6):, $\{\delta\}$ denotes the nodal degrees of freedom; $\{F\}$ denotes the overall nodal force vector;

$[K]$ and denotes the overall stiffness matrix of the structure.

(4) Solve for unknown degrees of freedom, unit stress-strain and collate calculation results.

3. Modelling Ideas

In the process of analyzing the force performance of the bridge, the use of appropriate numerical methods can significantly reduce the amount of computation, and at the same time can accurately simulate the performance of the bridge in the actual working condition. If we discretize all the components of the bridge, including the main arch rib steel pipe, concrete, girders and cross braces, etc., using plate and shell elements or block elements, it will lead to too many degrees of freedom in the calculation, which will make the whole calculation process too time-consuming, the data collation work becomes extremely heavy, and the modification of the model also becomes difficult. In addition, due to the complexity of the calculation results, its intuition will be greatly reduced, thus making this method not practical enough in practical applications.

On the other hand, if we choose to use spatial beam elements to simulate the arch ribs while using plate and shell elements to simulate the beams, although this method can simplify the computational process to a certain extent, it will still face some problems. Specifically, this method will lead to an excessive number of nodes, which in turn makes the whole calculation process slow and inefficient. Therefore, Midas Civil software was used to construct a spatial finite element model of the whole bridge for the structural analysis of the bridge. In order to more accurately simulate the stresses on the bridge deck system, the spatial beam lattice method was used for modelling. In this model, the bridge deck is divided into four longitudinal girders in the transverse direction and further subdivided into sixteen rows of transverse girders in the longitudinal direction to ensure the accuracy of the analysis.

In order to fully capture the mechanical behavior of each component of the bridge, key elements such as boom, arch ribs, steel-tube concrete, longitudinal girders, and K-braces were modelled using space truss and beam units. The connections between these components are treated as rigid connections to ensure that they can work together when under stress, so as to more realistically reflect the mechanical properties of the actual structure. The whole bridge model contains 655 nodes and 884 units, which together constitute the 3D spatial structure of the bridge. The spatial finite element model of the whole bridge, as shown in Fig. 1.

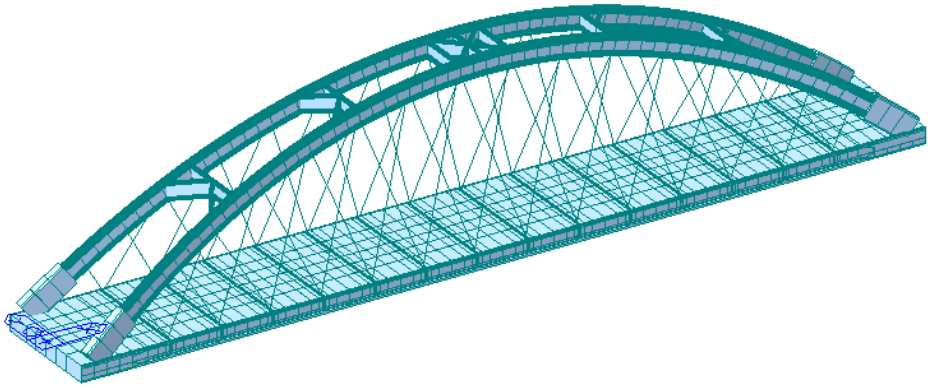

Figure 1 Spatial finite element model

4. Results and analyses of spatial finite element calculations considering the construction process

4.1 Displacement of beam body at each stage

Figure 2 shows the vertical displacements of the beam body at each stage. The deflections of the tie beams are all 0 before removing the full-height braces, so the vertical displacements of the beams under constant load are only selected as the research object after removing the full-height braces. After removing the full-load bracing of the beam, the vertical displacement curves of the beam at each stage under the action of the beam's self-weight, prestressing force and boom force were in the shape of 'M', and the vertical displacements of the middle beam and the side beams at the same stage were in good agreement, but due to the influence of the beam by the transverse prestressing force, the vertical displacement of the middle beam was slightly smaller than that of the side beams, and the vertical displacement of the middle beam at three construction stages was slightly smaller than that of the side beams. However, due to the influence of transverse prestressing, the vertical downward displacement of the middle girder is slightly smaller than that of the edge girder, and the difference between the vertical displacements of the middle girder and the edge girder in the three stages of the construction is distributed in the range of 1.121mm~1.65mm, and the maximum value of vertical upward displacement occurs in the 20m and 112m of the middle girder in the downward direction of the bridge after the completion of the demolition of full-height bracing with the maximum value of 6.519mm, and the maximum value of the vertical downward displacement of the girder occurs in the mid-span of the edge girder after the completion of the ten years of the Xuzhou ten years, and the maximum value of the -23.404 mm.

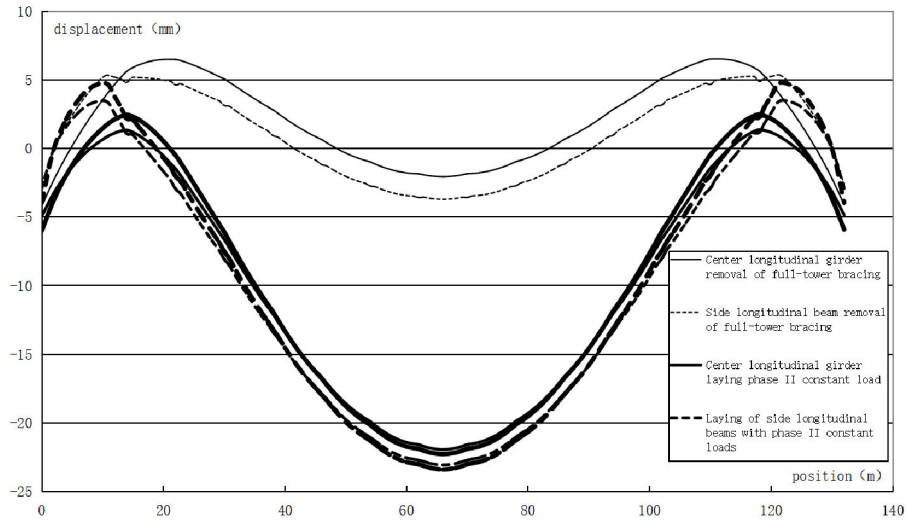

Fig. 2 Vertical displacements of beams in various stages

4.2 Accumulated stresses in the second phase of constant load stage of the girders

Figure 3 shows the upper edge stress and lower edge stress curves of the longitudinal beam after the completion of the second phase of constant load laying, respectively. From the figure, it can be seen that: after the completion of the laying of the second phase of constant load, the curve trend of the middle longitudinal beam and the side longitudinal beam basically coincides with the vast majority of the region of the beam body is in the state of compression, and only in the girder beam end cross-section of the upper edge of the very small tensile stresses, the maximum tensile stress is 1.62Mpa, to meet the design requirements of the tensile strength of the C50 concrete. The maximum compressive stress was -7.63Mpa, which occurred at the lower edge of the cross section at 13.2m and 118.8m of the longitudinal girder.

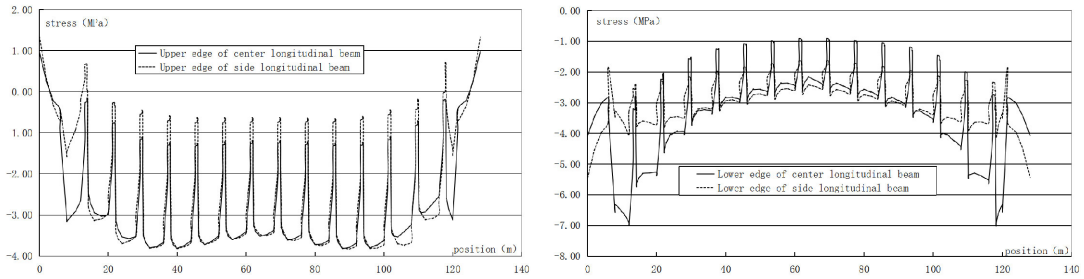

Fig. 3 Stress curves of longitudinal beams after completion of constant load in the second phase of paving

4.3 Deflection and force state under live loads

Figure 4 shows the deflection envelope of the tie beam under live load. From the figure, it can be seen that under live load: the deflection envelopes of the middle tie beam and the side tie beam under live load basically coincide with each other, the maximum deflection of the tie beam downward is -22.10mm, and the maximum deflection of the tie beam upward is 7.42mm; the maximum deflection or minimum deflection of the middle tie beam and the side tie beam is not more than 1mm, and the deflection ratio of the tie beam is 1/5792, which is far enough to meet the requirement of the stiffness.

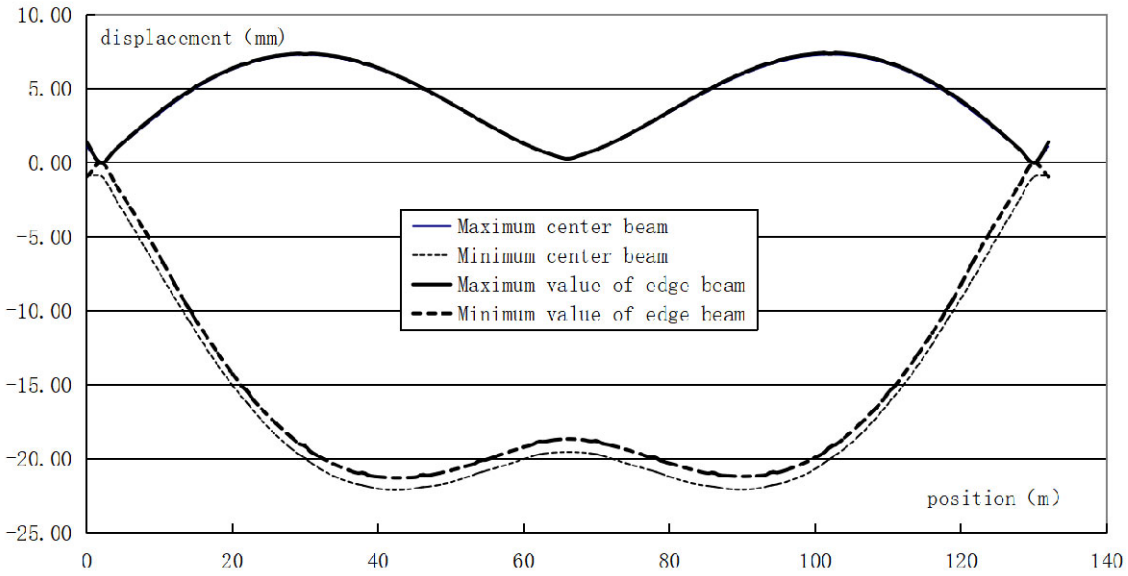

Fig. 4 Deflection envelope of the beam under live loads

Fig. 5 shows the stresses in the center tie beam and the stress envelope of the side tie beam under live load. From the figure, it can be seen that under live load, the maximum compressive stresses of the longitudinal girder

in the center tie beam and the edge tie beam are -1.56MPa and -1.08MPa respectively, the maximum compressive stresses of the center tie beam occur at 24m and 104m along the bridge, and the maximum compressive stresses of the edge tie beams occur in the end of the girder. The stress envelope curves of the center and side girders are in good agreement, and the stresses in each cross-section of the girders are relatively small.

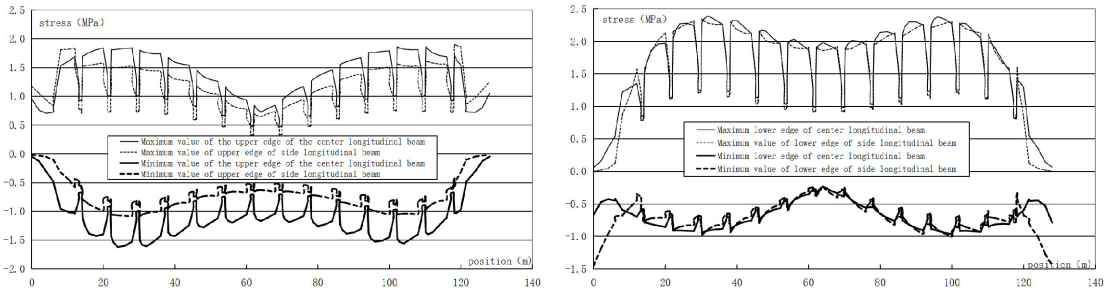

Fig. 5 Stress envelope of the beam under live loads

4.4 Force analysis of beam under constant load + live load

Figure 6 shows the envelope diagrams of the center tie beam and side tie beam under constant load + live load, from the figure, it can be seen that the deflection envelope diagrams of the center tie beam and side tie beam under constant load + live load match well, the maximum downward displacement of the longitudinal girder is -41.73mm, which occurs at the mid-span of the girder, and the maximum upward displacement of the longitudinal girder is 7.12mm, which occurs near the junctions of the No.1, No.2 booms and the No.1‘, No.2’ booms with the girder body. ' near the junction of boom no. 1 and beam body. The deflection-to-span ratio of the girder is less than 1/3085, which is far enough to satisfy the stiffness requirement.

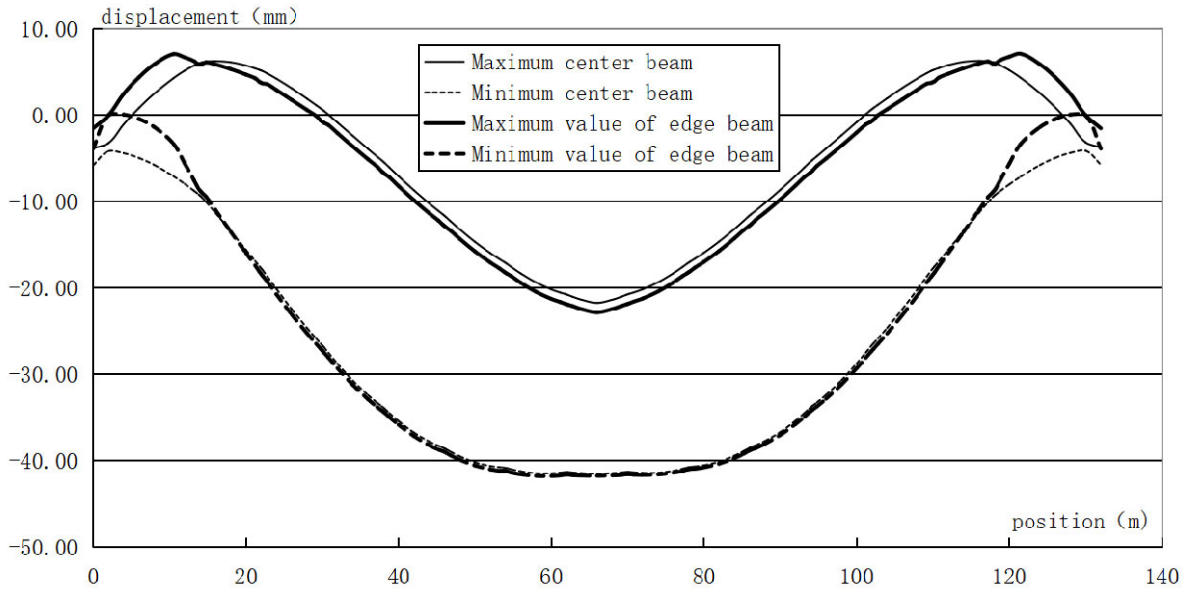

Fig. 6 Deflection envelope of the girder under constant load + live load

Under the joint action of constant load and live load, the stress envelope curves of the middle tie beam and side tie beam in the bridge direction are shown in Fig. 7. It can be seen intuitively from the figure that the stress envelope curves of the upper and lower edges of the middle and side tie beams are in good agreement, and the maximum tensile of the beam is 1.84MPa, which is smaller than the design value of tensile strength of C50 concrete, the maximum tensile stress occurs in the intersection of the beam and the bearing, and the maximum compressive stress is -6.42MPa, which occurs at the two ends of the beam. The maximum tensile stress occurs at the intersection of the beam and the support, and the maximum compressive stress of the beam is -6.42 MPa,

which occurs at the ends of the beam.

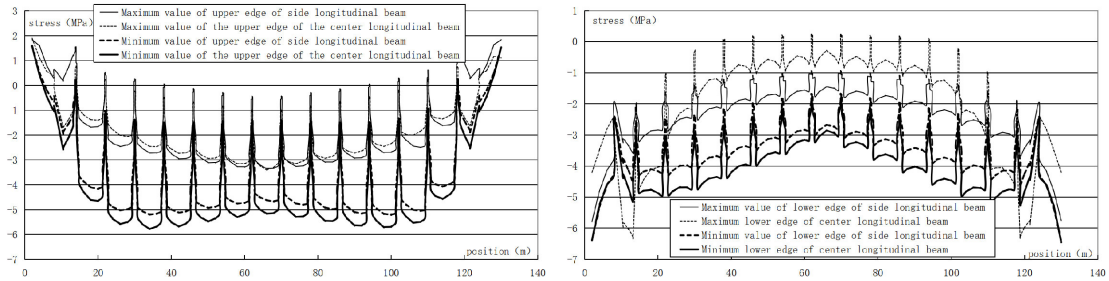

Fig. 7 Stress envelope of the beam under constant + live loads

5. Analysis of spatial effects

5.1 Unevenness of transverse distribution of vertical displacement of beam body

Vertical displacement of the beam body has some difference in the transverse direction, at the time of completion (constant load), the vertical displacement of the beam body span in the middle and side longitudinal beams are -21.95mm, -23.07mm respectively, and the downward deflection of the middle longitudinal beam is smaller than that of the side longitudinal beams, while under the action of separate live load, the vertical displacement of the beam body span in the middle and side longitudinal beams are -19.54mm, -18.65mm respectively, and the downward deflection of the middle longitudinal beams is larger than that of the side longitudinal beams. The vertical displacements of the middle and side longitudinal beams in the span under constant load and the most unfavorable live load are -41.49mm and -41.73mm respectively, and the deflection of the middle longitudinal beam is smaller than that of the side longitudinal beams.

5.2 Unevenness of transverse distribution of longitudinal stress in girder body

There is a certain gap in the transverse distribution of the girder longitudinal stress, for example: at the time of completion (constant load), the compressive stress in the span of the girder, the top plate of the side longitudinal girder is -4.12Mpa, -3.99Mpa, the top plate of the middle longitudinal girder is larger than the side longitudinal girder, the bottom plate of the middle and side longitudinal girder is -2.28Mpa, -2.62Mpa, the top plate of the middle longitudinal girder is smaller than the side longitudinal girder; individually, the compressive stress in the span of the girder under live load is -41.49mm, -41.73mm. Under the action of live load, the compressive stress in the span of the girder is -0.72Mpa, -0.54Mpa, the compressive stress in the top plate of the middle longitudinal girder is greater than that of the side longitudinal girder, and the bottom plate of the middle and side longitudinal girder is -0.29Mpa, -0.32Mpa, and the compressive stress in the top plate of the middle longitudinal girder is smaller than that of the side longitudinal girder; under the action of the combination of constant load and live load, the compressive stress in the span of the girder is -4.97Mpa, -4.97Mpa, -4.62Mpa, -4.97Mpa, -2.62Mpa. Under the combined force of constant load and live load, the compressive stress in the span of the girder is -4.97Mpa and -4.48Mpa respectively, the compressive stress in the top plate of the middle longitudinal girder is larger than that in the side longitudinal girder, and the bottom plate of the middle and side longitudinal girder is -2.25Mpa and -2.61Mpa respectively, the compressive stress in the top plate of the middle longitudinal girder is smaller than that in the side longitudinal girder.

5.3 Transverse Stresses in the Beam Body

The maximum stresses in the beams of 128NBTAB after the completion of removal of the full beam bracing, the completion of laying of the second constant, and the completion of the decade of creep are shown in Table 1.

Table 1
Maximum stress in crossbeam (MPa)

Load	Removal of tie beam full support complete	Laying Erheng completed	Xu change ten years complete
Side Crossbeam	-6.68	-7.74	-7.48
Crossbeam at 1/4 span	-4.51	-4.14	-4.10
Crossbeam at 1/2 span	-4.34	-3.91	-3.92

5.4 Lateral displacement of arch ribs

The maximum lateral displacement of the arch rib of 128NBTAB under constant load, least favorable live load and constant load + live load is shown in Table 2.

Table 2
Maximum transverse displacement of arch rib (mm)

Load	Maximum lateral displacement (mm)
Constant load	4.31
Most unfavorable live load	2.95
Constant load + least favorable live load	5.53

5.5 Lateral component force of the boom and lateral unbalance force at the lifting point

The transverse component force of the boom and the transverse unbalance force of the lifting point of 128NBTAB under constant load, most unfavorable live load and constant load + most unfavorable live load are shown in Table 3.

Table 3
Lateral component force of boom and lateral unbalance force of lifting point (KN)

Load		Constant load	Most unfavorable live load	Constant load + least favorable live load
Lateral component force of the boom	Max	249.9	69.0	295.7
	Min	131.1	24.9	156.1
Lateral unbalance force at lifting point	Max	381.0	137.7	510.5
	Min	340.0	70.7	451.7

5.6 Evaluation of space effect

In view of the above analyses can be obtained, space the bridge in the vertical load, the beam vertical displacement and longitudinal stress transverse distribution slightly uneven, transverse stress is generally smaller than the longitudinal stress, mainly caused by the transverse prestressing force and the transverse component force of the boom. The arch rib also has a slight transverse displacement in addition to the vertical displacement.

6. Conclusion

In this paper, finite element analysis was carried out on the deformation and force state of the bridge under constant load, live load, and combination of live load + constant load, and the vertical displacement, transverse displacement and boom force of the beam under constant load, and the envelope diagram of the displacement and stress under live load, and combination of live load + constant load, etc.; the deformation and force state of the bridge was evaluated, and the spatial effect was investigated. The following conclusions are drawn:

(1) The maximum vertical deflection of the girder under the most unfavorable live load is -22.10mm, and the deflection-to-span ratio is 1/5792; the stiffness meets the specification requirements and has a large margin.

(2) The displacement of the girder body is dominated by the vertical displacement, and the longitudinal and

transverse displacements are very small. Under the action of main force combination in the whole construction process and operation stage, the vertical displacement of the girder body is the largest in the span, -23.07mm under the action of constant load, and -41.73mm under the action of constant load + the most unfavorable combination of live load, and the longitudinal and transverse displacements of the girder body are small, which are mainly caused by the longitudinal and transverse prestressing.

(3) The longitudinal unbalance force of 32.6-602.2KN and the transverse unbalance force of 451.7-510.5KN of the two booms acting on the girders at each lifting point of each side of the bridge were all occurred under the action of the combination of the constant load and the most unfavorable live load.

(4) The unevenness of stress distribution in the transverse direction is not too obvious in each cross-section of the girder body in the crossover direction. Under the combined force of constant load and the most unfavorable live load, the compressive stress in the bottom plate at the girder end is -6.38Mpa at the outer side of the girder body and -6.42Mpa at the center.

(5) The lateral distribution of vertical displacement of the beam body is slightly uneven. The vertical displacement of beam body in span under the most unfavorable live load is -18.65mm at the edge of the beam and -19.54mm at the center of the beam.

(6) From the above conclusions, it can be seen that the strength and stiffness of the bridge meet the requirements, and the displacement and stress mainly occur in the vertical plane, and the spatial effect is not serious.

7. Reference

[1] LIU Wen-shuo, DAI Gong-lian, HE Xu-hui. Sensitive factors research for track-bridge interaction of Long-span X-style steel-box arch bridge on high-speed railway [J].Journal of Central South University》, 2013, 20(11):3314-3323.

[2] Zhao Yueyu, Lao Wenquan, Feng Rui, et al. Analysis of the effect of internal inclination angle on the mechanical properties of steel-pipe concrete lifting arches[J]. Highway Traffic Science and Technology, 2007, 24(3):56-58.

[3] LIU Zhenyu, SUN Chao, CHEN Baochun. Analysis of dynamic characteristics of steel-pipe concrete lifting arch[J]. Highway Traffic Science and Technology,2001.

[4] ZHOU Qian, FENG Pengcheng, HU Lifei, et al. Design of structural system of large-span double continuous steel-tube concrete arch bridge[J]. World Bridge, 2024, 52(2):101-106.

[5] LI Zite, WANG Genhui, FAN Jiang, et al. Analysis of stress performance of large-span top-bearing steel-tube concrete arch bridge[J]. Journal of Railway Engineering, 2024, 41(1):32-38.

[6] WAN Chengfu, ZENG Wenli. Research on key technology of demolition of multi-span continuous steel-tube concrete arch bridge[J]. Chinese and foreign highways, 2024, 44(2):164-173.

[7] Feng Jia. Seismic response analysis of top-bearing steel-tube concrete arch bridges in deep-cut canyons[J]. Highway Traffic Technology, 2024(6).

[8] ZHOU Qian, FENG Pengcheng, ZHOU Jianting, et al. Analysis of concrete de-vacuuming in tubes of steel-pipe concrete arch bridges under inhomogeneous temperature field[J]. Bridge Construction, 2024, 54(1):103-109.